

1 **Topological relationship-based flow direction modeling:**
2 **stream burning and depression filling**

3 **Chang Liao¹, Tian Zhou¹, Donghui Xu¹, Zeli Tan¹, Gautam Bisht¹, Matthew**
4 **Cooper¹, Darren Engwirda², Hong-Yi Li³, L. Ruby Leung¹**

5 ¹Atmospheric Sciences and Global Change, Pacific Northwest National Laboratory, Richland, WA, USA

6 ²T-3 Fluid Dynamics and Solid Mechanics Group, Los Alamos National Laboratory, Los Alamos, NM,

7 USA

8 ³University of Houston, Houston, TX, USA

9 **Key Points:**

- 10 • We use topological relationships in adaptive stream burning.
11 • We use a mesh-independent approach to conduct depression filling.
12 • The model produces several flow routing parameters including flow direction.

Corresponding author: Chang Liao, chang.liao@pnnl.gov

13 Abstract

14 Flow direction modeling consists of (1) an accurate representation of the river net-
15 work and (2) digital elevation model (DEM) processing to preserve characteristics with
16 hydrological significance. In part 1 of our study, we presented a mesh-independent ap-
17 proach to representing river networks on different types of meshes. This follow-up part
18 2 study presents a novel DEM processing approach for flow direction modeling. This ap-
19 proach consists of (1) a topological relationship-based hybrid breaching-filling method
20 to conduct stream burning for the river network and (2) a modified depression removal
21 method for rivers and hillslopes. Our methods minimize modifications to surface eleva-
22 tions and provide a robust two-step procedure to remove local depressions in DEM. They
23 are mesh-independent and can be applied to both structured and unstructured meshes.
24 We applied our new methods to the Susquehanna River Basin with different model con-
25 figurations. The results show that topological relationship-based stream burning and depression-
26 filling methods can reproduce the correct river networks, providing high-quality flow di-
27 rection and other characteristics for hydrologic and Earth system models.

28 Plain Language Summary

29 Flow direction and several other flow routing attributes are important inputs for
30 hydrologic models. Existing methods have several limitations, including only support-
31 ing rectangle mesh systems. In this study, we extend our topology-based river network
32 representation method to define flow direction and other attributes. With its new fea-
33 tures, our method can be used to generate high-quality flow routing parameters for hy-
34 drologic models.

35 1 Introduction

36 Flow direction field and flow routing parameters are key inputs to hydrologic and
37 Earth system models. To generate these inputs, flow direction models must consider hy-
38 drologic features including river networks and land surfaces across different scales (Tarboton,
39 2003; Yamazaki et al., 2009; Wu et al., 2012; Li et al., 2013; Liao et al., 2019). Because
40 the spatial discretizations, including the mesh system and spatial resolution of hydro-
41 logic and Earth system models, generally do not match the real-world hydrologic fea-
42 tures, the modeled flow direction field and flow routing parameters are always concep-
43 tual. Limitations remain on how to represent different hydrologic features in the flow di-
44 rection field across different scales. Most existing methods are limited to rectangle mesh
45 systems (Nobre et al., 2011; Wu et al., 2011; McGehee et al., 2016; Engwirda & Liao, 2021).
46 Currently, two primary methods exist to model flow direction field and flow routing pa-
47 rameters. This paper is the second part of a topological relationship-based flow direc-
48 tion modeling series. Readers are referred to our earlier work for additional background
49 information (Liao, Zhou, Xu, Cooper, et al., 2022).

50 The first flow direction modeling method is used at the regional/watershed scale,
51 with flow direction often generated through terrain analysis (Tarboton, 2003; Esri Wa-
52 ter Resources Team, 2011; Liao et al., 2020). In terrain analysis, both (1) “stream burn-
53 ing”, a technique to enforce flow direction by modifying a raster Digital Elevation Model
54 (DEM) at and near the river channel using a user-provided vector dataset, and (2) “de-
55 pression removal”, a technique to remove local depressions within DEM so water can flow
56 out of the domain, are used to pre-process the DEM (Hellweger & Maidment, 1997; Barnes
57 et al., 2014; Lindsay, 2016b). After the DEM is modified, the flow direction can be de-
58 fined using the elevation differences (e.g., the direction with the largest elevation drop).
59 Many models have been developed for stream burning and depression removal since the
60 1980s (Hellweger & Maidment, 1997; Wesseling et al., 1997; Graham et al., 1999; Wang
61 & Liu, 2006; Barnes et al., 2014). The stream burning method was extensively discussed

62 in our earlier study(Liao, Zhou, Xu, Barnes, et al., 2022) and other literature(Lindsay,
63 2016b).

64 The major limitation in existing stream-burning models is their aggressive mod-
65 ifications to the river (and the riparian zone) elevations. These modified elevations di-
66 rectly alter the calculation of slope, an important flow routing parameter. The modifi-
67 cations are needed because the models treat the vector-based river networks as a binary
68 mask to lower the elevations. Unlike stream burning, depression removal does not require
69 a vector-based river network dataset as input and can be carried out before or after stream
70 burning. Depending on how elevation is modified, depression removal can be classified
71 into (1) depression filling, which increases the elevation of the depression(Barnes et al.,
72 2014), and (2) depression breaching, which breaches a path from the depression towards
73 the domain boundary. Depression filling is more computationally efficient but suffers from
74 aggressive elevation modifications. Depression breaching does not have the aggressive
75 modification issue, but it suffers from computational complexity(Lindsay, 2016b).

76 While stream burning and depression removal are different techniques, they are closely
77 connected. A cell’s elevation may be modified by both techniques so that stream burn-
78 ing may alter the result of depression removal or vice versa. Several studies have tried
79 to combine stream burning and depression removal within a unified workflow to obtain
80 consistent results(Saunders, 2000; Liao, Zhou, Xu, Barnes, et al., 2022). However, pro-
81 ducing a hydrologic-simulation-ready DEM and its associated flow direction remains chal-
82 lenging as a well-established elevation manipulation scheme does not exist(Lindsay, 2016b,
83 2016a). Previous research proposed an alternative hybrid breaching filling method to min-
84 imize the modification to both river and land elevations(Lindsay, 2016b). The method
85 uses a revised priority flood approach to fill the land cell depressions and river network
86 topological relationships to breach river cell depressions.

87 The second flow direction modeling method is used at a continental or global scale.
88 As discussed in our part 1 study, it is often referred to as the “upscaling” method (e.g.,
89 the Dominant River Tracing (DRT) model) because it uses high spatial resolution datasets
90 (e.g., results from the raster DEM-based method) as guidance to define the coarse res-
91 olution (around 10 km to 200 km) cell-to-cell flow direction(Fekete et al., 2001; Davies
92 & Bell, 2009; Wu et al., 2011). Because this method often assumes that there is always
93 one major river channel within each large-scale mesh cell, the flow direction field is gen-
94 erally equivalent to the river networks. Because the upscaling method relies on high spa-
95 tial resolution datasets, it does not require additional stream burning or depression re-
96 moval. It derives flow routing parameters through fine-scale data synthesis.

97 Similar to the river network representation methods, existing flow direction mod-
98 els at both regional and global scales are limited to the rectangle mesh systems, although
99 some algorithms can be extended to other mesh systems(Barnes et al., 2014). Model de-
100 velopment based on unstructured meshes has become an emerging area of interest in hy-
101 drologic and Earth system models. In addition to the three advantages discussed in our
102 part 1 study, model development based on unstructured meshes also address several lim-
103 itations of traditional hydrologic models, including high latitude spatial distortion(Liao
104 et al., 2020).

105 To the authors’ knowledge the HexWatershed model, a hexagon mesh-based wa-
106 tershed delineation model, is the only flow direction model that includes both stream burn-
107 ing and depression removal and can be extended to a fully unstructured mesh framework
108 as of this writing(Liao et al., 2020). This study extends our part 1 study(Liao, Zhou, Xu,
109 Cooper, et al., 2022), describing a topological relationship-based river network represen-
110 tation method to introduce topological relationship-based stream burning and depression-
111 filling algorithms within the HexWatershed model. We upgrade the HexWatershed model
112 to a fully mesh-independent framework(Liao et al., 2020; Liao, Zhou, Xu, Barnes, et al.,
113 2022; Liao & Cooper, 2022). Part 2 of the study is organized as follows. We first intro-

114 duce the model algorithms. We then apply the updated model to the same coastal wa-
 115 tershed used in the part 1 study, the Susquehanna River Basin (SRB), with different model
 116 configurations and evaluate the model performance against several characteristics and
 117 datasets (e.g., elevation, slope, and drainage area). Finally, we discuss the method’s lim-
 118 itations and future applications in hydrologic and Earth system models.

119 2 Methods

120 2.1 Overview of HexWatershed

121 HexWatershed (v1.0/2.0) was originally designed as a hexagonal mesh-based wa-
 122 tershed delineation model(Liao et al., 2020). Later on, we introduced stream burning to
 123 improve the flow direction and stream network representation at coarse spatial resolu-
 124 tions (Figure S1)(Liao, Zhou, Xu, Barnes, et al., 2022). Because the core stream burn-
 125 ing algorithm within HexWatershed v2.0 is based on a rasterization-based method, the
 126 model is subject to the same limitations as existing methods.

127 2.2 What’s new in HexWatershed

128 In HexWatershed v3.0, we introduced topological relationship-based stream burn-
 129 ing and revised depression-filling algorithms. The overall workflow of HexWatershed v3.0
 130 is similar to earlier versions, with the major difference being the use of topological re-
 131 lationships (Figure 1). Additional watershed characteristics including travel distance (the
 132 flow direction-based distance between each cell and its watershed outlet) are also mod-
 133 eled.

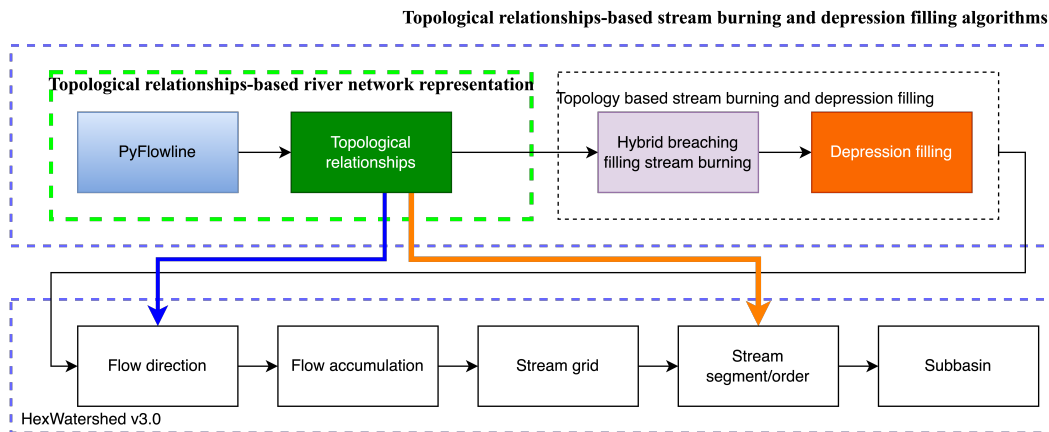


Figure 1: Workflow of the HexWatershed v3.0 model with the topological relationship-based stream burning and depression filling algorithms. Rectangles inside the green dashed rectangle are the part 1 study topological relationship-based river network representation using the PyFlowline model, which produces the topological relationships information (green rectangle). The topological relationships are used by the hybrid breaching filling stream burning algorithm (light purple rectangle), followed by the revised depression filling algorithm (orange rectangle). The topological relationships are also used by the flow direction algorithm (blue arrow) and stream segment/order definition algorithms (orange arrow).

1334 We will first introduce the topological relationship-based stream burning and depression-
1335 filling algorithms before providing details of the mesh-independent framework.

1336 **2.3 Topological relationship-based stream burning and depression fill-** 1337 **ing**

1338 The topological relationship-based stream burning and depression-filling algorithms
1339 process cell elevations using a two-step approach. First, the model processes river cells
1340 and their riparian zone land cells using a hybrid breaching filling stream burning algo-
1341 rithm. In this step, each river cell may be modified more than once because of the breach-
1342 ing algorithm. Second, the model processes the remaining land cells using a revised pri-
1343 ority flood depression filling algorithm. Because the second step does not modify the re-
1344 sults of the first step, this approach generates a consistent depression-free DEM with river
1345 networks burnt in.

1346 *2.3.1 Hybrid breaching-filling stream burning*

1347 The PyFlowline simulation from our part 1 study produces a JavaScript Object
1348 Notation (JSON) file that contains the neighbor and downstream information (if appli-
1349 cable) of each mesh cell(Liao et al., 2020). The hybrid breaching filling stream burning
1350 algorithm uses this information to adaptively fill or breach river cell elevation. The stream
1351 burning algorithm in our model is essentially a depression removal (both filling and breach-
1352 ing) algorithm specifically designed for river networks.

1353 Similar to our earlier study(Liao, Zhou, Xu, Barnes, et al., 2022), the algorithm
1354 reversely searches and adjusts river cells from the outlet toward the headwater. With-
1355 out significantly decreasing the outlet elevation, it adjusts the elevation of a depression
1356 river cell using either filling or breaching based on the elevation difference between the
1357 depression and a user-provided threshold. For example, if the absolute value of depres-
1358 sion is lower than the user-provided threshold, a filling is applied. Otherwise, breaching
1359 is applied. Figure 2 provides a one-dimensional example.

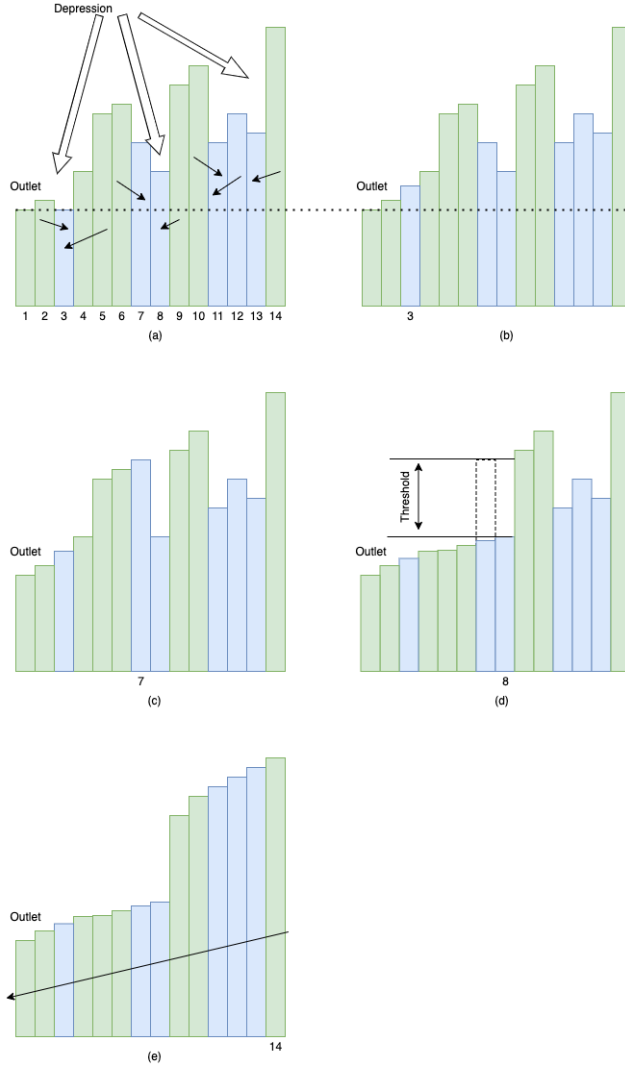


Figure 2: Illustration of the hybrid breaching filling stream burning algorithm. (a) is the original river cell elevation profile, which is the same as that in Figure S1. Each cell is marked with an index, which is also the order/step it is processed. (b) Because the depression between cells 2 and 3 is less than the user-provided threshold (e.g., 5 m), cell 3's elevation is increased by a gentle slope (e.g., 1%). (c) Similarly, cell 7's elevation is increased. (d) Because the difference between the updated cells 7 and 8 exceeds the threshold, cell 8's elevation is unchanged, while cell 7 and its downstream cells are breached if needed. (e) shows the resulting river cell elevation profile.

160 This algorithm runs recursively until all the river segments/reaches are processed
 161 (Figure S2). Because stream order information is also available from the PyFlowline sim-
 162 ulation, different parameters are used for different upstream channels when a river cell
 163 is a confluence. For example, a lower percentage (e.g., 1%) is used for high-order rivers,
 164 and a higher value (e.g., 2%) is used for low-order rivers. After the river cells are pro-
 165 cessed, the land cells' elevations in their riparian zones are increased if needed.

166 The topological relationships feature can also be turned off (Table S1). This con-
 167 verts the river networks from the PyFlowline JSON file to a binary mask. As a result,

168 the model runs in a traditional rasterization-based stream burning method and only ap-
 169 plies depression filling in the river cells and their riparian zone land cells.

170 **2.3.2 Revised priority-flood depression filling**

171 Unlike our earlier study(Liao, Zhou, Xu, Barnes, et al., 2022) which processes both
 172 river and land cells in the depression filling algorithm, this new revised algorithm pushes
 173 the river cells and their riparian zone land cells into the queue without changing their
 174 elevations. As a result, the priority queue does not form a “closed boundary”.

175 **2.4 Mesh-independent framework**

176 To support unstructured mesh systems(Ringler et al., 2013; Sahr, 2015; Engwirda,
 177 2017), HexWatershed v3.0 includes several changes. First, it supports all mesh systems
 178 from the mesh-independent PyFlowline model(Liao, Zhou, Xu, Cooper, et al., 2022). How-
 179 ever, the definitions of neighboring cells in PyFlowline and HexWatershed v3.0 are not
 180 always the same (Text S1). For example, a rectangle cell in PyFlowline has only 4 neigh-
 181 bors. In contrast, the same cell may have 8 neighbors (4 face neighbors + 4 vertex neigh-
 182 bors) in HexWatershed (Text S1).

183 Second, in a projected coordinate system (PCS), flow accumulation is often rep-
 184 resented using the total number of upslope cells that contribute to the current cell. The
 185 total drainage area can be calculated by multiplying the flow accumulation by the cell
 186 area, which is a constant. In an unstructured mesh, the cell area is not constant. To re-
 187 solve this, we use the geodesic area of each cell when calculating the flow accumulation.

188 Third, HexWatershed v3.0 supports continental to global scale simulation, which
 189 is enabled by the design of the PyFlowline model. PyFlowline allows for multi-outlet mod-
 190 eling to generate multiple river basin networks within a single mesh. Based on this, HexWa-
 191 tershed v3.0 performs stream burning and depression filling for multiple watersheds in
 192 one simulation.

193 **3 Model application**

194 **3.1 Study area and data**

195 We applied the model to the same study area used in our part 1 study, the Susque-
 196 hanna river basin (Figure S3). We use the same baseline datasets from our part 1 study.
 197 However, the user-provided river networks in this study represent the conceptual river
 198 networks produced from our part 1 study. Additionally, we also obtained the DEM dataset
 199 from the United States National Elevation Dataset (NED). Spatial datasets and maps
 200 were produced using Python packages including Matplotlib and GDAL(Hunter, 2007;
 201 Gillies & others, 2007; GDAL/OGR contributors, 2019; Liao, 2022b; Liao & Cooper, 2022;
 202 Liao, 2022a).

203 **3.2 Model setup**

204 To evaluate the performance of the HexWatershed v3.0, we ran the model under
 205 different configurations with case indices used for illustrations (Tables S1 and 1). The
 206 resolutions and case indices differ from those in our part 1 study.

Table 1: Simulation configurations with case indices. The illustrations and analyses all use the same indices.

Mesh	5 km		40 km	
	Without topology	With topology	Without topology	With topology
Latlon	1	2	3	4
Square	5	6	7	8
Hexagon	9	10	11	12
MPAS (3 ~ 10 km)	13	14		

207 For structured meshes, we ran 2 different spatial resolutions (5 km and 40 km). For
 208 unstructured mesh, i.e., the Model for Prediction Across Scales(MPAS) mesh, we used
 209 a variable resolution mesh with cell lengths varying from 3 km to 10 km. To demonstrate
 210 the effect of the topological relationship-based stream burning algorithm, we ran two sim-
 211 ulations (without and with the topological relationships) for each resolution. The sup-
 212 plimentary materials contain the high-resolution meshes (overlapped with flow direction)
 213 of Cases 2, 6, 10, and 14 (Figures S4-S7).

214 3.3 Results and analysis

215 Although the new algorithms affect many results, we only present major watershed
 216 characteristics often used by hydrologic and Earth system models, such as surface slope
 217 and flow direction.

218 3.3.1 Surface elevation

219 The modeled surface elevations with and without topological relationships exhibit
 220 significant differences near river cells. When the topological relationships feature is turned
 221 off, the modeled river cell elevations dramatically decrease due to the large threshold (i.e.,
 222 100 m) applied. As a result, the river networks are also visible (e.g., Cases 1, 5, and 9
 223 in Figure 3). The dramatic modification is also widespread from the headwater to the
 224 outlet.

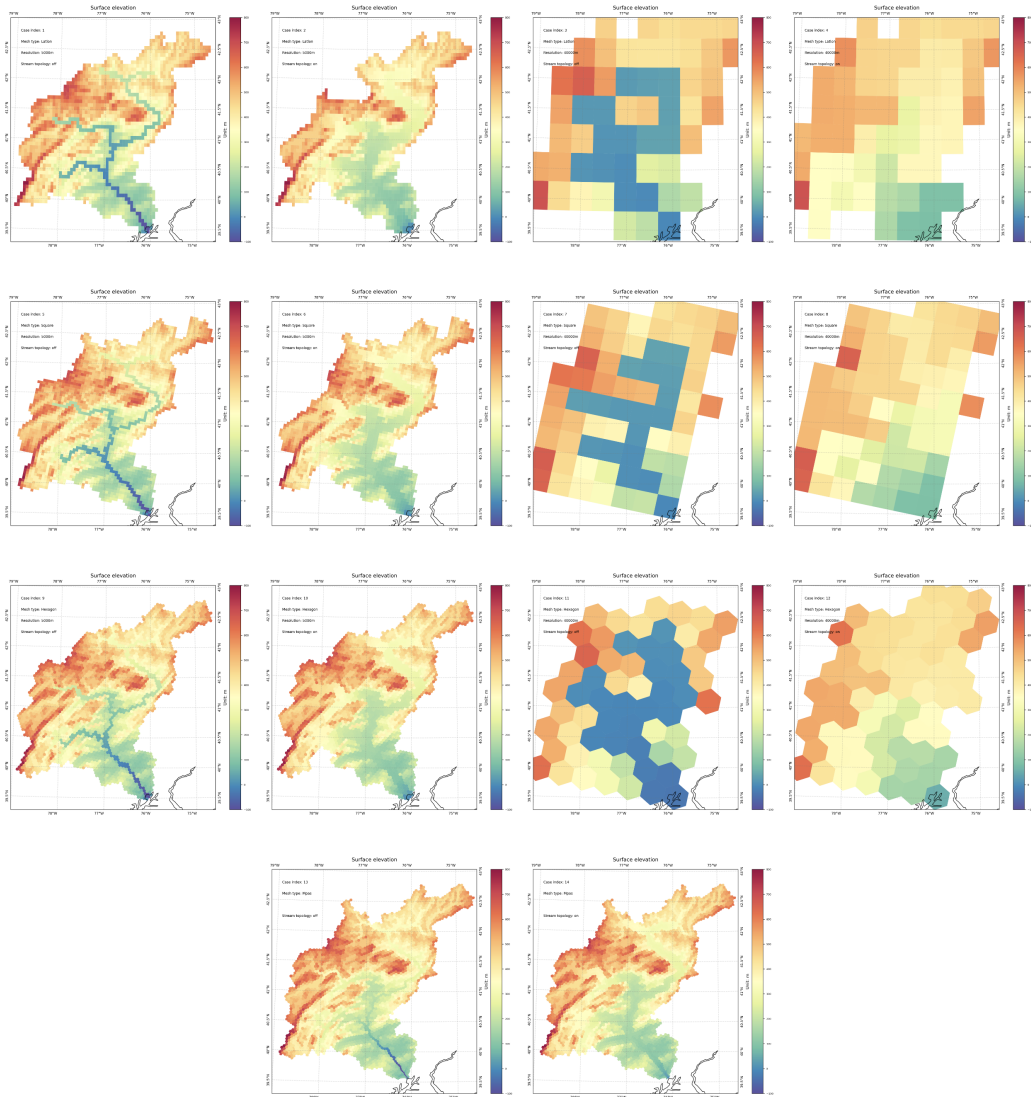


Figure 3: The spatial distributions of modeled surface elevation in Cases 1 to 14 (unit: m)(Table 1). Because the topological relationships feature is turned off in cases with odd indices (e.g., 1, 3, 5, and 7), the river cell elevations are much lower than the corresponding cases with even indices (e.g., 2, 4, 6, and 8).

225 In contrast, when the topological relationships feature is turned on, modeled river
 226 cell elevations are closer to their riparian zone cell elevations (e.g., Cases 2, 6, 10, and
 227 14 in Figure 3).

228 We also extracted the elevation profiles from the watershed outlet to a United States
 229 Geological Survey (USGS) gauge site (Site ID: 01497842) on the main channel. The re-
 230 sults show that when the topological relationships feature is turned on, the model is able
 231 to produce more realistic elevation gradients along the channel (Figure 4). However, the
 232 modeled elevations are still overestimated compared to the NED datasets (Text S2).

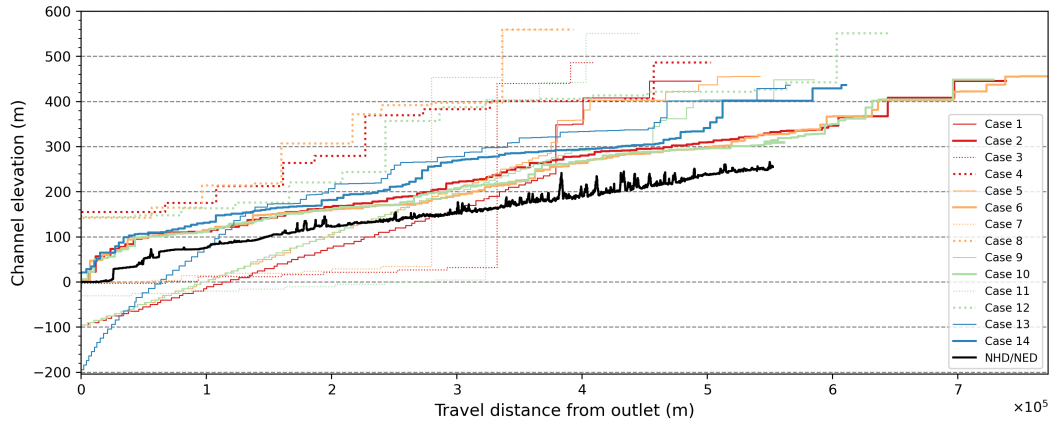


Figure 4: River elevation (m) from the outlet to the main channel upstream USGS gage site 01497842 (travel distance in m) for Cases 1 to 14 and the National Hydrography Dataset(NHD)/NED (Table 1). The x-axis is the travel distance from the outlet, and the y-axis is the elevation. The black line represents the elevation profile from the NED datasets. Different cases have a different number of data points due to resolution differences. The NED datasets are not depression-free.

233
234
235

The topological relationships feature also has a significant impact on the distributions of domain-wide channel elevations (Figure 5). In general, the average river channel elevations are much higher with the feature turned on than when it is turned off.

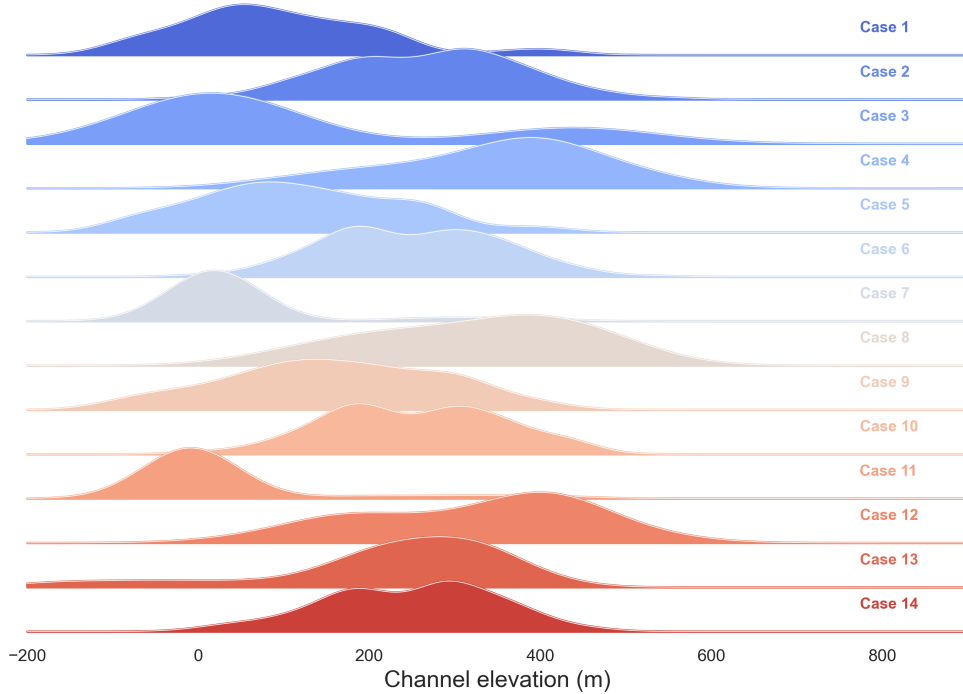


Figure 5: Density functions of the river channel elevation (m) from Cases 1 to 14 (Table 1).

236

3.3.2 Surface slope

237

238

239

Because the model calculates the between-cell slope from the depression-free surface elevation, the spatial patterns of the modeled slope with and without topological relationships are generally similar. Significant differences can appear near the river cells.

240

241

242

The density functions of the channel slope show that the average channel slope is smaller when the topological relationships feature is turned on than when it is turned off (Figure S8). This is consistent with the elevation profiles (Figure 4).

243

244

245

Because the river cell elevations substantially decrease when the topological relationships feature is turned off, the slopes between the river cells and their riparian zone cells are much larger than when this feature is turned on (Figure 6).

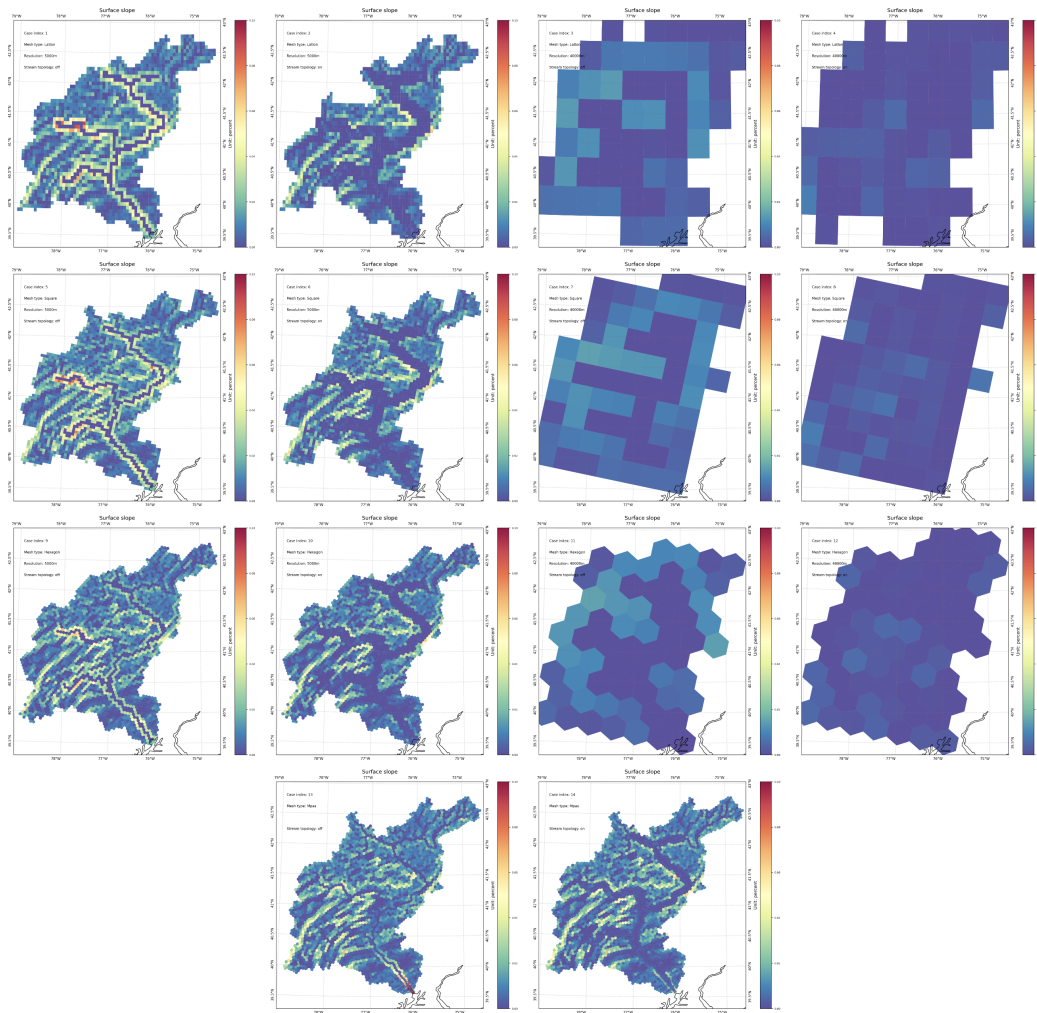


Figure 6: Spatial distributions of the modeled surface slope from Cases 1 to 14 (Table 1). Because the river cell elevations in cases with odd indices (e.g., 1, 3, 5, and 7) are lower than in cases with even indices (e.g., 2, 4, 6, and 8), the slopes near these cells are much larger.

246 The density functions of the riparian zone slopes show that the average riparian
 247 zone slope is more than 10 times larger when the topological relationships feature is turned
 248 off than when it is turned on. Their distributions are less affected by mesh types and res-
 249 olutions when it is turned on (Figure 7).

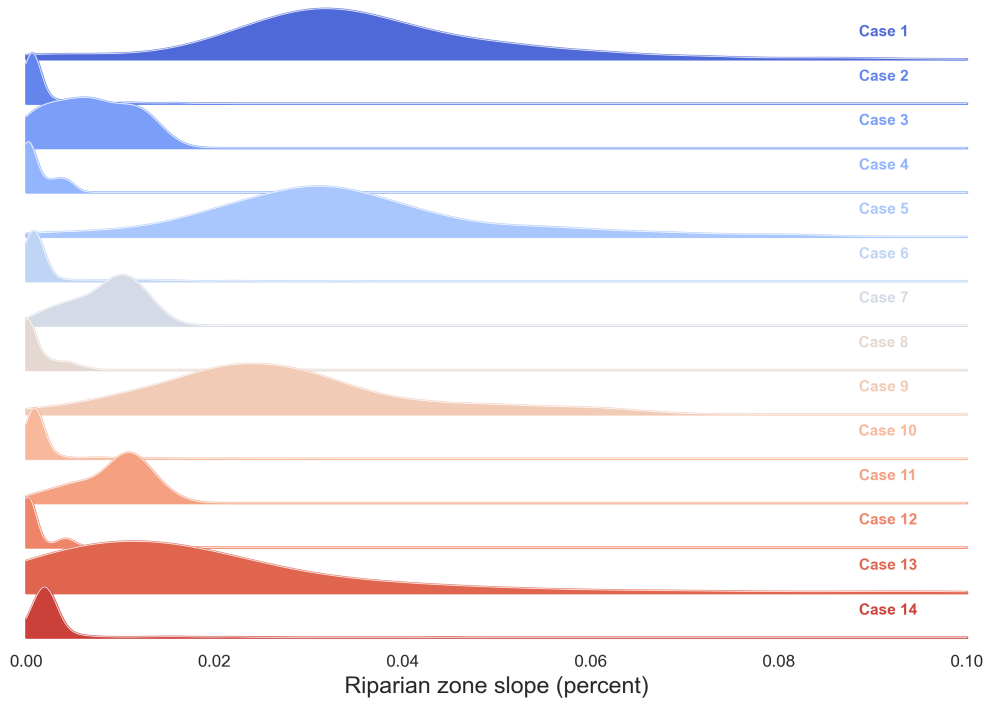


Figure 7: Density functions of the river riparian zone slope (percent) from Cases 1 to 14 (Table 1).

250 **3.3.3 Flow direction**

251 When the topological relationships feature is turned off, the model cannot repro-
 252 duce flow direction fields that precisely follow the user-provided river networks, especially
 253 at coarse resolutions (e.g., Cases 3, 7, and 11 in Figure 8). Specifically, the modeled flow
 254 direction fields cannot resolve river meanders and confluences.

255 In contrast, when the topological relationships feature is turned on, the modeled
 256 flow direction fields exactly overlap the user-provided river networks regardless of mesh
 257 type and resolution (e.g., Cases 2, 4, and 14 in Figure 8).

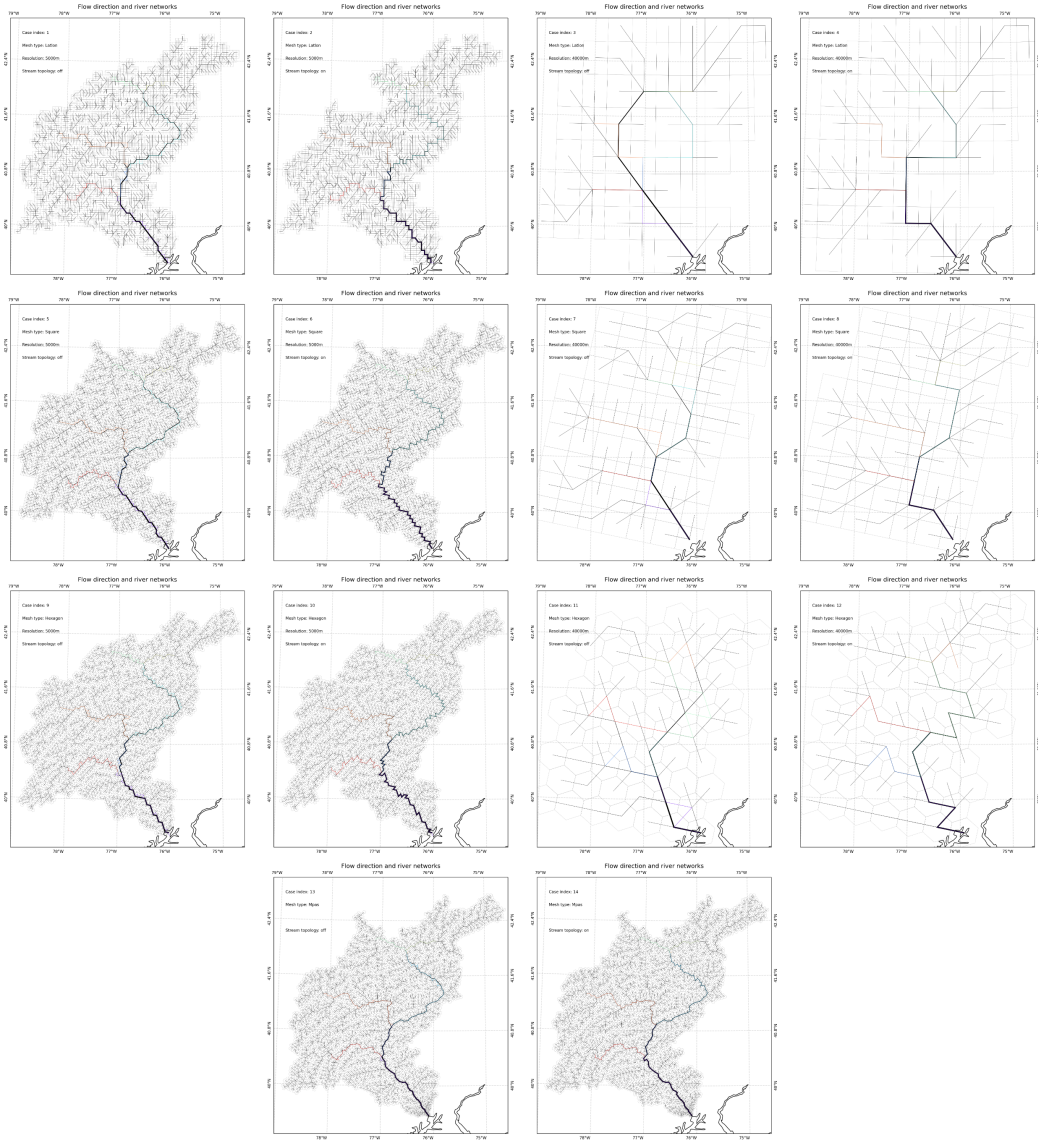


Figure 8: Modeled flow direction fields from Cases 1 to 14 (Table 1). The black line features represent flow direction fields with the drainage area scaled as the line thickness. The colored line features are the user-provided river networks from the PyFlowline simulation. When the topological relationships feature is turned on, the modeled flow direction fields are consistent with the user-provided river networks.

258

3.3.4 Drainage area

259

260

261

262

263

Because drainage area is calculated based on cell area and flow direction, the modeled drainage area varies with mesh type and resolution. When the topological relationships feature is turned off, the spatial patterns of modeled drainage areas from different meshes are similar at high resolutions. However, they differ significantly at coarse resolutions (e.g., Cases 3 and 6 in Figure 9).

264

265

266

In contrast, the drainage area spatial patterns from different meshes are very similar when the topological relationships feature is turned on across all tested resolutions (e.g., Cases 4, 8, and 12 in Figure 9).

267 At high mesh resolution, turning on the topological relationships feature better cap-
 268 tures flow direction near river channels (e.g., Cases 13 and 14 in Figure 9).

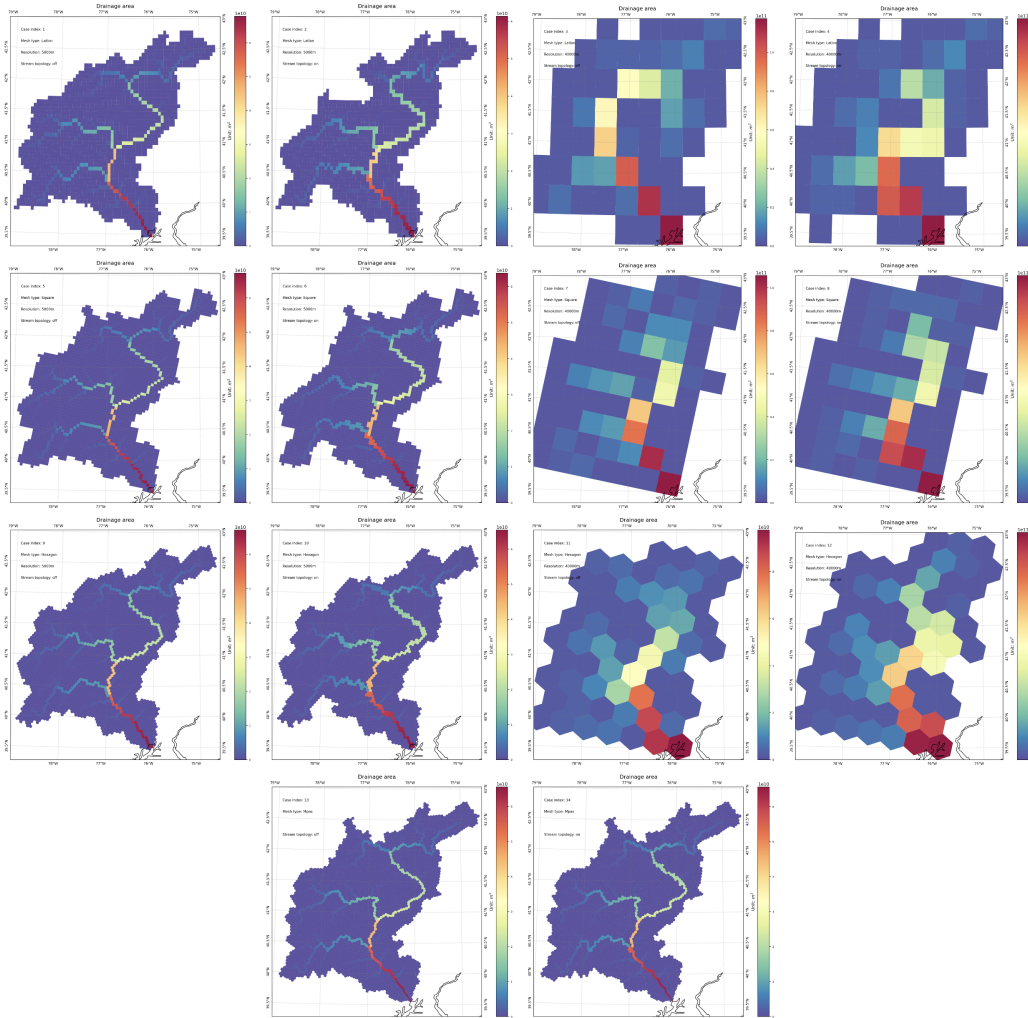


Figure 9: The modeled drainage area from Cases 1 to 14 (m^2)(Table 1).

269 All cases underestimated the total drainage area by 5% to 10% at high spatial res-
 270 olution. This is primarily caused by missing portions at the upper boundary (e.g., Cases
 271 2 and 10 in Figure 9). The numbers of cells in all cases suggest that the MPAS mesh in-
 272 cludes more cells than other meshes due to its refinement near the watershed outlet (Fig-
 273 ure S9).

274 In contrast, all cases overestimated the total drainage area by as much as 30% (Fig-
 275 ure 10) at coarse spatial resolution. This is primarily because the model frequently in-
 276 cludes cells that are partially within the watershed (less than 50% in total area) during
 277 the stream-burning process.

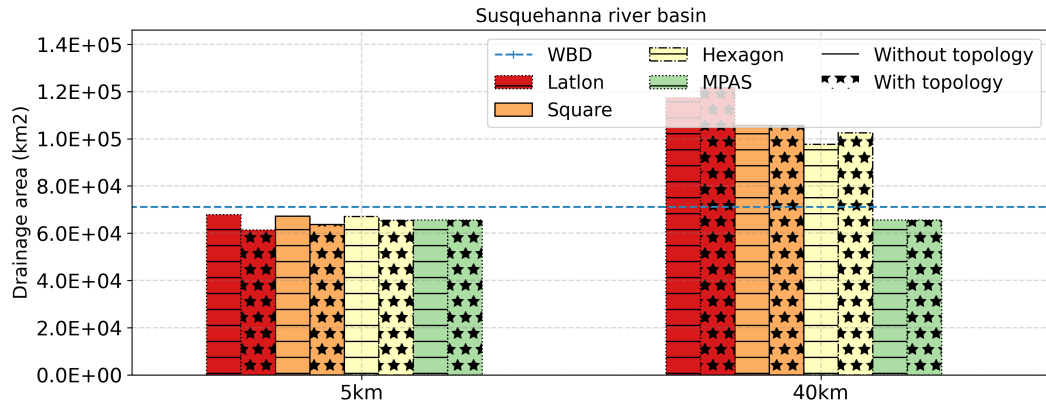


Figure 10: Drainage area at the watershed outlet from Cases 1 to 14 (km^2) (Table 1). The x-axis is the mesh resolution (5km and 40km), and the y-axis is the drainage area (km^2). The dashed line is the reference drainage area from the Watershed Boundary Dataset (WBD). MPAS-based cases are plotted in both resolutions.

278

3.3.5 *Travel distance*

279

280

281

282

283

284

Similar to drainage area, travel distance depends on flow direction and is calculated using accumulated cell center-to-center distance. The modeled travel distances have similar spatial patterns at high resolutions regardless of mesh type and resolution. The topological relationship feature does not have a significant impact on travel distance. This is because a cell can have a similar travel distance even with different flow directions (Figure S10).

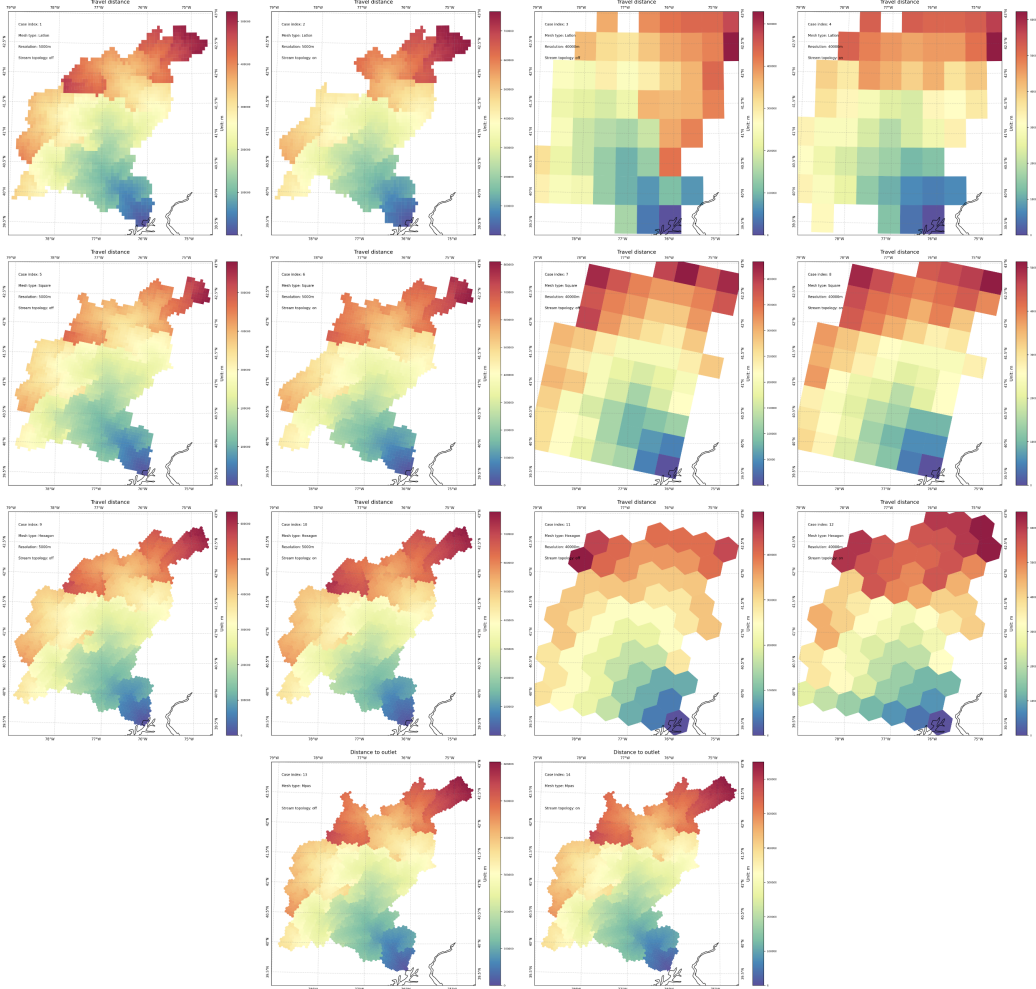


Figure 11: The modeled travel distances from Cases 1 to 14 (Table 1).

285 The scatter plot between the observed and modeled travel distances suggests that
 286 the model can reasonably capture the travel distance, especially when the topological
 287 relationship feature is turned on. First, when this feature is turned off at the high spatial
 288 resolution, the flow direction often takes shortcuts and the model often underesti-
 289 mates the travel distance (e.g., Cases 1, 5, 9, and 13 in Figure 12). In contrast, when it
 290 is turned on and the flow direction precisely follows the river channel, the modeled travel
 291 distances are larger and maybe even be greater than observations (e.g., Cases 2, 6, 10,
 292 and 14). Second, compared with structured meshes, MPAS mesh-based cases underes-
 293 timate travel distance because the river cells are aligned with real-world river channels.
 294 Third, a strong correlation ratio exists between the observed and modeled travel distances
 295 when the topological relationship feature is turned on. This ratio depends on the mesh
 296 type. For example, the ratio for the structured latlon, square, and hexagon meshes are
 297 1.04, 1.04, and 1.03, respectively. Finally, Case 14 performs similarly to the DRT model
 298 at 1/16 degree resolution (~ 7 km) near the watershed outlet. The DRT model uses the
 299 actual flowlines to represent the travel distance(Wu et al., 2011).

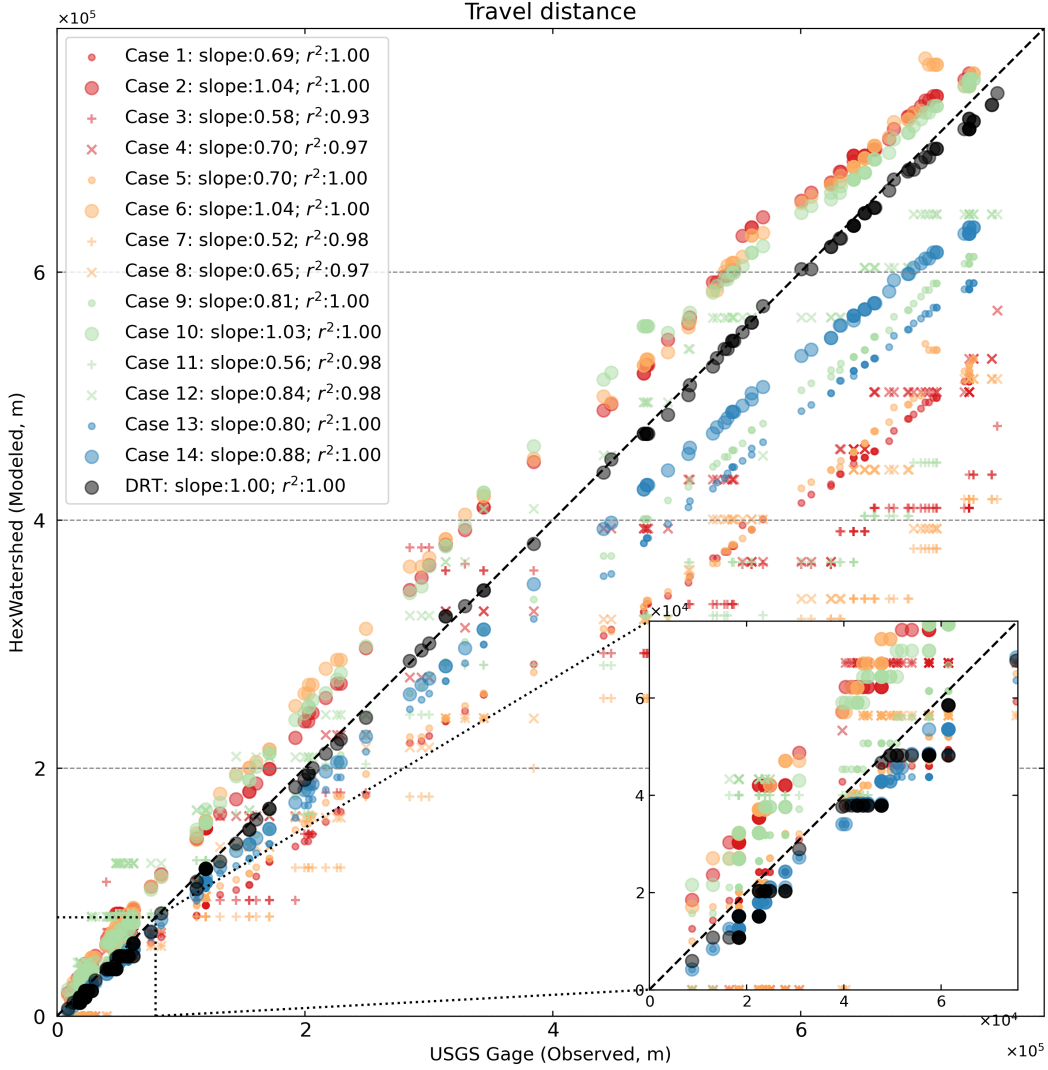


Figure 12: Comparison between the USGS measured and modeled travel distances at 160 NWIS sites from Cases 1 to 14 and the DRT datasets (Table 1). The black circles represent the DRT model datasets at 1/16 degree resolution.

300

4 Discussion

301

4.1 Importance of topological relationships in stream burning

302

303

304

305

306

307

308

309

310

Model simulations from Cases 1 to 14 demonstrate that the topological relationship-based stream burning can minimize modification to river and land elevations. This is because the adaptive hybrid breaching filling algorithm uses topological relationships to adjust elevations on demand (Figure 3)(Lindsay, 2016b). As a result, the updated DEM can be used to directly model river channel and riparian zone slopes that meet hydrologic model requirements. However, the comparison between modeled DEM and NED datasets suggests that the model parameters, i.e., the filling ratio and breaching threshold, should be tested to improve further model performance (Figure 4). The flow direction algorithm considers both the topological relationships and elevation gradient, al-

311 lowing it to define flow direction fields that are consistent with the user-provided con-
 312 ceptual river networks (Figures S4-S7).

313 However, because these capabilities depend on the topological relationships mod-
 314 eled by PyFlowline, the limitations from the part 1 study propagate into this study.

315 4.2 Depression filling

316 Unlike the method from our earlier study(Liao, Zhou, Xu, Barnes, et al., 2022), our
 317 new method separates stream burning and depression filling into two steps and signif-
 318 icantly simplifies the workflow.

319 First, the new method demonstrates that, if carefully designed, we can conduct full-
 320 domain depression removal sequentially to include different hydrologic features (e.g., lakes,
 321 rivers, and land) without introducing additional model complexity. The results remain
 322 consistent after the final step.

323 Second, because stream burning minimizes the modification to the river (and its
 324 riparian zone) elevations, the improvements will also improve depression filling for the
 325 remaining land cells.

326 4.3 Watershed characteristics across scales

327 The hydrologic processes in hydrologic and Earth system models are not at the same
 328 spatial scales as the mesh resolutions. As a result, representing watershed characteris-
 329 tics across scales is critical. Our simulation cases suggest that some characteristics, such
 330 as the travel distance, can be reconstructed from the conceptual travel distance by a scale
 331 factor (Figure 12). However, reconstruction remains challenging for other characteris-
 332 tics. For example, river segment and river order information can differ from case to case.
 333 Even in the same case, the modeled stream segment and order outputs can vary from
 334 the user-provided values because of the flow accumulation threshold(Lin et al., 2021).
 335 In some scenarios, preserving these values is preferred to maintain consistency (the or-
 336 ange arrow in Figure 1). Another example is drainage area, as all cases either underes-
 337 timate or overestimate the total drainage area. This is mainly caused by the missing por-
 338 tions or the partially included/excluded cells at basin margins (Figures 9 and S9).

339 4.4 Limitations

340 This study has a few limitations:

- 341 1. Currently, we only consider the immediate neighbors as the river channel buffer
 342 zone in the stream burning algorithm, which means the single-cell resolution de-
 343 termines the buffer zone width. An adaptive buffer zone width that includes more
 344 than immediate neighbors is needed when the riparian zone width is larger than
 345 the mesh resolution.
- 346 2. The elevation gradient near the river mouth is generally smoother compared to
 347 the vicinity of the headwaters (Figure 4). As a result, the filling and breaching pa-
 348 rameters should be adaptive, considering the mesh resolution and distance to the
 349 watershed outlet. In some cases, a dam may alter the elevation profile. These pa-
 350 rameters should also depend on the location of the river channel (Figure 4).
- 351 3. The model should include other hydrologic features such as watershed boundary
 352 and (endorheic) lakes in the workflow. For example, it is possible to include wa-
 353 tershed boundaries in the mesh generation process to allow the model to improve
 354 the drainage area without missing the marginal areas. Similarly, we should include
 355 lakes in the mesh generation and depression removal processes to consider fill-spill
 356 scenarios(Barnes et al., 2020).

357 5 Conclusions

358 In this study, we extended our part 1 study to develop a mesh-independent topo-
 359 logical relationship-based flow direction model (HexWatershed v3.0). We applied the model
 360 in different configurations to the Susquehanna River Basin. The results show that our
 361 model minimizes modification to the river and land elevations and produces high-quality
 362 flow direction fields and other flow routing parameters. We suggest that hydrologic and
 363 Earth system models with a flow routing component should adopt our method, especially
 364 for unstructured mesh-based simulations.

365 Acknowledgments

366 This research was funded as part of the multi-program, collaborative Integrated
 367 Coastal Modeling (ICoM) project and the Interdisciplinary Research for Arctic Coastal
 368 Environments (InterFACE) project through the Department of Energy, Office of Sci-
 369 ence, Biological and Environmental Research program, Earth and Environment Systems
 370 Sciences Division, Earth System Model Development (ESMD) program area. The data
 371 used for model simulations can be downloaded through the USGS website (<https://www.usgs.gov/national-hydrography>). The HexWatershed model can be installed as a
 372 Python package (<https://github.com/changliao1025/pyhexwatershed>) (Liao, 2022a).
 373 The data and code used in this paper are available from https://github.com/DOE-ICoM/liao-et-al_2022_hexwatershed_james. A portion of this research was performed us-
 374 ing PNNL Research Computing at Pacific Northwest National Laboratory. PNNL is op-
 375 erated for DOE by Battelle Memorial Institute under contract DE-AC05-76RL01830.
 376
 377

378 Conflict of Interest

379 The authors certify that they have NO affiliations with or involvement in any or-
 380 ganization or entity with any financial interest (such as honoraria; educational grants;
 381 participation in speakers' bureaus; membership, employment, consultancies, stock own-
 382 ership, or other equity interest; and expert testimony or patent-licensing arrangements),
 383 or non-financial interest (such as personal or professional relationships, affiliations, knowl-
 384 edge or beliefs) in the subject matter or materials discussed in this manuscript.

385 References

- 386 Barnes, R., Callaghan, K. L., & Wickert, A. D. (2020). Computing water flow
 387 through complex landscapes, Part 3: Fill-Spill-Merge: Flow routing in de-
 388 pression hierarchies. *Earth Surface Dynamics Discussions*, 1–22. doi:
 389 10.5194/esurf-9-105-2021
- 390 Barnes, R., Lehman, C., & Mulla, D. (2014). Priority-flood: An optimal depression-
 391 filling and watershed-labeling algorithm for digital elevation models. *Comput-
 392 ers & Geosciences*, 62, 117–127. doi: 10.1016/j.cageo.2013.04.024
- 393 Davies, H. N., & Bell, V. A. (2009). Assessment of methods for extracting low-
 394 resolution river networks from high-resolution digital data. *Hydrological Sci-
 395 ences Journal*, 54(1), 17–28. doi: 10.1623/hysj.54.1.17
- 396 Engwirda, D. (2017). JIGSAW-GEO (1.0): locally orthogonal staggered unstruc-
 397 tured grid generation for general circulation modelling on the sphere. *Geosci-
 398 entific Model Development*, 10(6), 2117–2140.
- 399 Engwirda, D., & Liao, C. (2021, 10). 'Unified' Laguerre-Power Meshes for Cou-
 400 pled Earth System Modelling. *Zenodo*. Retrieved from [https://zenodo.org/
 401 record/5558988](https://zenodo.org/record/5558988) doi: 10.5281/ZENODO.5558988
- 402 Esri Water Resources Team. (2011). *Arc Hydro Tools - Tutorial* (Tech. Rep.).
- 403 Fekete, B. M., Vorosmarty, C. J., & Lammers, R. B. (2001). Scaling gridded river
 404 networks for macroscale hydrology: Development, analysis, and control of

- 405 error. *Water Resources Research*, 37(7), 1955–1967.
- 406 GDAL/OGR contributors. (2019). *Geospatial Data Abstraction software Library*.
407 Retrieved from <https://gdal.org>
- 408 Gillies, S., & others. (2007). *Shapely: manipulation and analysis of geometric ob-*
409 *jects*. Retrieved from <https://github.com/Toblerity/Shapely>
- 410 Graham, S. T., Famiglietti, J. S., & Maidment, D. R. (1999). Five-minute, 1/2°, and
411 1° data sets of continental watersheds and river networks for use in regional
412 and global hydrologic and climate system modeling studies. *Water Resources*
413 *Research*, 35(2), 583–587.
- 414 Hellweger, F., & Maidment, D. (1997). AGREE-DEM surface
415 reconditioning system. Online at <http://www.ce.utexas.edu/prof/maidment/gishydro/ferdi/research/agree/agree.html> (last accessed
416 March 3, 2005).
- 417
- 418 Hunter, J. D. (2007). Matplotlib: A 2D graphics environment. *Computing in Science*
419 *and Engineering*, 9(3), 90–95. doi: 10.1109/MCSE.2007.55
- 420 Li, H., Wigmosta, M. S., Wu, H., Huang, M., Ke, Y., Coleman, A. M., & Leung,
421 L. R. (2013). A physically based runoff routing model for land surface and
422 earth system models. *Journal of Hydrometeorology*, 14(3), 808–828. doi:
423 10.1175/JHM-D-12-015.1
- 424 Liao, C. (2022a, 4). *HexWatershed: A mesh independent flow direction model for*
425 *hydrologic models [Software]*. Zenodo. Retrieved from [https://doi.org/10](https://doi.org/10.5281/zenodo.6425881)
426 [.5281/zenodo.6425881](https://doi.org/10.5281/zenodo.6425881) doi: 10.5281/zenodo.6425881
- 427 Liao, C. (2022b, 3). *A lightweight Python package for Earth science [Software]*. Zen-
428 odo. Retrieved from <https://zenodo.org/record/6368652> doi: 10.5281/
429 ZENODO.6368652
- 430 Liao, C., & Cooper, M. (2022, 4). *Pyflowline a mesh-independent river network gen-*
431 *erator for hydrologic models [Software]*. Zenodo. Retrieved from [https://doi](https://doi.org/10.5281/zenodo.6407299)
432 [.org/10.5281/zenodo.6407299](https://doi.org/10.5281/zenodo.6407299) doi: 10.5281/zenodo.6407299
- 433 Liao, C., Tesfa, T., Duan, Z., & Leung, L. R. (2020). Watershed delineation
434 on a hexagonal mesh grid. *Environmental Modelling & Software*, 128,
435 104702. Retrieved from [http://www.sciencedirect.com/science/article/](http://www.sciencedirect.com/science/article/pii/S1364815219308278)
436 [pii/S1364815219308278](http://www.sciencedirect.com/science/article/pii/S1364815219308278) doi: 10.1016/j.envsoft.2020.104702
- 437 Liao, C., Zhou, T., Xu, D., Barnes, R., Bisht, G., Li, H.-Y., ... Engwirda, D.
438 (2022). Advances in hexagon mesh-based flow direction modeling. *Advances in*
439 *Water Resources*, 104099. doi: 10.1016/j.advwatres.2021.104099
- 440 Liao, C., Zhou, T., Xu, D., Cooper, M., Engwirda, D., Li, H.-Y., & Leung, L. R.
441 (2022). Topological relationships-based flow direction modeling: mesh-
442 independent river networks representation.
- 443 Liao, C., Zhuang, Q., Leung, L. R., & Guo, L. (2019). Quantifying Dissolved Or-
444 ganic Carbon Dynamics Using a Three-Dimensional Terrestrial Ecosystem
445 Model at High Spatial-Temporal Resolutions. *Journal of Advances in Modeling*
446 *Earth Systems*, 11(12), 4489–4512. doi: 10.1029/2019MS001792
- 447 Lin, P., Pan, M., Wood, E. F., Yamazaki, D., & Allen, G. H. (2021). A new vector-
448 based global river network dataset accounting for variable drainage density.
449 *Scientific data*, 8(1), 1–9.
- 450 Lindsay, J. B. (2016a). Efficient hybrid breaching-filling sink removal methods for
451 flow path enforcement in digital elevation models. *Hydrological Processes*,
452 30(6), 846–857. doi: 10.1002/hyp.10648
- 453 Lindsay, J. B. (2016b). The practice of DEM stream burning revisited. *Earth Sur-*
454 *face Processes and Landforms*, 41(5), 658–668. doi: 10.1002/esp.3888
- 455 Mcgehee, R., Li, L., & Poston, E. (2016, 10). National Water Center Innovators Pro-
456 gram Summer Institute Report. Chapter 5: The Modified HAND Method. In
457 (pp. 37–45).
- 458 Nobre, A. D., Cuartas, L. A., Hodnett, M., Rennó, C. D., Rodrigues, G., Silveira,
459 A., & Saleska, S. (2011). Height Above the Nearest Drainage—a hydrologically

- 460 relevant new terrain model. *Journal of Hydrology*, 404(1-2), 13–29.
- 461 Ringler, T., Petersen, M., Higdon, R. L., Jacobsen, D., Jones, P. W., & Maltrud,
462 M. (2013). A multi-resolution approach to global ocean modeling. *Ocean*
463 *Modelling*, 69, 211–232. doi: 10.1016/j.ocemod.2013.04.010
- 464 Sahr, K. (2015). *DGGRID version 6.2 b: User documentation for discrete global grid*
465 *software*.
- 466 Saunders, W. (2000). Preparation of DEMs for use in environmental modeling anal-
467 ysis. *Hydrologic and Hydraulic Modeling Support. Redlands, CA: ESRI*, 29–51.
- 468 Tarboton, D. G. (2003). Terrain analysis using digital elevation models in hydrolog-
469 ogy. In *23rd esri international users conference, san diego, california* (Vol. 14).
470 Citeseer.
- 471 Wang, L., & Liu, H. (2006). An efficient method for identifying and filling surface
472 depressions in digital elevation models for hydrologic analysis and modelling.
473 *International Journal of Geographical Information Science*, 20(2), 193–213.
- 474 Wesseling, C. G., Van Deursen, W. P. A., & De Wit, M. (1997). Large scale catch-
475 ment delineation: a case study for the River Rhine basin. *Geographical Infor-*
476 *mation*, 1, 487–496.
- 477 Wu, H., Kimball, J. S., Li, H., Huang, M., Leung, L. R., & Adler, R. F. (2012). A
478 new global river network database for macroscale hydrologic modeling. *Water*
479 *resources research*, 48(9). doi: 10.1029/2012WR012313
- 480 Wu, H., Kimball, J. S., Mantua, N., & Stanford, J. (2011). Automated upscaling
481 of river networks for macroscale hydrological modeling. *Water Resources Re-*
482 *search*, 47(3). doi: 10.1029/2009WR008871
- 483 Yamazaki, D., Oki, T., & Kanae, S. (2009). Deriving a global river network map
484 and its sub-grid topographic characteristics from a fine-resolution flow direc-
485 tion map. *Hydrology and Earth System Sciences*, 13(11), 2241–2251. doi:
486 10.5194/hess-13-2241-2009